



**PES University, Bengaluru**  
(Established under Karnataka Act No. 16 of 2013)  
100-ft Ring Road, Bengaluru-560085, Karnataka, India

# **Enhancement of Low-Quality Underwater Images by using an Enhancement Algorithm**

*By*

**Sathvik Srinivas (PES1201800358)**  
**V. Ramakrishna Siddharth (PES1201800439)**  
**Surya Dutta (PES1201800674)**  
**Nikhil S. Khare (PES1201800552)**

under the guidance of

**Prof. Lavanya Krishna**  
Assistant Professor  
Department of Electronics and Communication Engineering  
PES University



**PES University, Bengaluru**  
(Established under Karnataka Act No. 16 of 2013)  
100-ft Ring Road, Bengaluru-560085, Karnataka, India

*Report on*

## **Enhancement of Low-Quality Underwater Images by using an Enhancement Algorithm**

*Submitted by*  
**Sathvik Srinivas (PES1201800358)**  
**V. Ramakrishna Siddharth (PES1201800439)**  
**Surya Dutta (PES1201800674)**  
**Nikhil S. Khare (PES1201800552)**

January - May 2021 and June - December 2021

under the guidance of

*Internal Guide*  
**Prof. Lavanya Krishna**  
Assistant Professor  
Department of Electronics and Communication Engineering  
PES University  
Bengaluru-560085

FACULTY OF ENGINEERING  
DEPARTMENT OF ELECTRONICS AND COMMUNICATION  
ENGINEERING  
PROGRAM: B.TECH



**PES University, Bengaluru**  
(Established under Karnataka Act No. 16 of 2013)  
100-ft Ring Road, Bengaluru-560085, Karnataka, India

# CERTIFICATE

*This is to certify that the Report entitled*  
**Enhancement of Low-Quality Underwater Images by using an  
Enhancement Algorithm**

*is a bona fide work carried out by*

**Sathvik Srinivas (PES1201800358)**  
**V. Ramakrishna Siddharth (PES1201800439)**  
**Surya Dutta (PES1201800674)**  
**Nikhil S. Khare (PES1201800552)**

In partial fulfillment for the completion of course work in the Program of Study B.Tech in Electronics and Communication Engineering, under rules and regulations of PES University, Bengaluru during the periods: January - May 2021 and June - December 2021. It is certified that all corrections/suggestions indicated for internal assessment have been incorporated in the report. The report has been approved as it satisfies the academic requirements in respect of Capstone project work.

*Signature with Date & Seal*

*Prof. Lavanya Krishna*  
*Internal Guide*

*Signature with Date & Seal*

*Dr. Anuradha M*  
*Chairperson*

*Signature with Date & Seal*

*Dr. B. K. Keshavan*  
*Dean - Faculty of Engg. & Technology*

Name and Signature of the Examiners:

- 1.
- 2.

# **DECLARATION**

We, Sathvik Srinivas, V. Ramakrishna Siddharth, Surya Dutta and Nikhil S. Khare, hereby declare that the report entitled “Enhancement of Low-Quality Underwater Images using an Enhancement Algorithm” is an original work done by us under the guidance of Prof. Lavanya Krishna, Assistant Professor, ECE Department and is being submitted in partial fulfillment of the requirements for completion of course work in the Program of Study, B.Tech in Electronics and Communication Engineering.

Place : Bengaluru

Date : September 25, 2021

Sl. no.	Name of the Student	Signatures
1	Sathvik Srinivas	
2	V. Ramakrishna Siddharth	V. Ramakrishna
3	Surya Dutta	
4	Nikhil S. Khare	

# Abstract

Since light undergoes absorption and scattering when it travels in water, images taken under water fall prey to colour distortion, fuzziness/haziness, underexposure, and colour cast. To alleviate these issues, we propose a novel Retinex-based enhancing approach aimed at enhancing low-quality underwater images. Firstly, the input image undergoes pre-processing, where a colour correction technique is employed to address the problem of colour distortion. This is followed by conversion of the input image from the RGB colour space to the CIE Lab colour space. Then, by means of the multi scale Retinex, the illumination component of the image is procured. Image dehazing algorithms, i.e., bright channel prior (BCP) and underwater dark channel prior (UDCP) algorithms are applied individually on the procured illumination component. The image gets enhanced and is then converted back to the RGB colour space from the CIE Lab colour space. The final enhanced image is obtained by performing histogram equalization on the enhanced RGB image. This is intended to make the output colour intensity more realistic. The efficacy of the algorithms are gauged by means of some image quality metrics. Compared to pre-existing techniques, our proposed method manages to effectively enhance images while keeping detail loss to a minimum.

# Acknowledgements

First and foremost, we would like to express our sincere gratitude to our Faculty Guide Prof. Lavanya Krishna for her continued support and encouragement throughout the development of this project. Without her guidance and assistance, our idea would not have come to fruition.

We are grateful to the Project Coordination Team composed of Prof. M. Rajasekar, Prof. Prajeesha and Prof. Sumanth Sakkara for efficiently organizing, managing and helping out with the entire process.

We convey our special thanks to Dr. Anuradha M, Chairperson, Department of Electronics and Communication Engineering, PES University, for all the knowledge and support that we received from the department.

We would like to thank Dr. B. K. Keshavan, Dean - Faculty of Engineering and Technology, PES University for his help.

We are deeply grateful to Dr. M. R. Doreswamy, Chancellor, PES University, Prof. Jawahar Doreswamy, Pro Chancellor, PES University and Dr. J. Suryaprasad, Vice-Chancellor, PES University for all the opportunities and enlightenment provided at every step of the way.

Finally, this project could not have been completed without the support and encouragement that we received from our parents and friends.

# Contents

<b>List of Figures</b>	<b>vi</b>
<b>List of Tables</b>	<b>vii</b>
<b>1 Introduction</b>	<b>1</b>
<b>2 Project Flow</b>	<b>2</b>
2.1 Flow of Literature Review . . . . .	2
2.2 Flow of Implementation . . . . .	3
<b>3 Literature Survey</b>	<b>4</b>
3.1 The General Dark Channel Prior Algorithm . . . . .	4
3.2 Underwater Dark Channel Prior Algorithm . . . . .	6
3.3 The Bright Channel Prior Algorithm . . . . .	7
3.4 Histogram Equalization . . . . .	9
3.5 Rayleigh Distribution based enhancement . . . . .	10
3.6 Integrated Colour Model . . . . .	11
3.7 Unsupervised Colour Correction Method . . . . .	12
3.8 The Retinex model . . . . .	13
3.8.1 The Single Scale Retinex . . . . .	15
3.8.2 The Multi Scale Retinex . . . . .	17
<b>4 Flow of the Technique proposed</b>	<b>19</b>
<b>5 Working Principle</b>	<b>20</b>
5.1 Pre-Processing Steps . . . . .	20
5.1.1 Colour Correction . . . . .	20
5.1.2 Conversion of the RGB image to Lab . . . . .	21
5.2 Implementation . . . . .	22
5.3 Post-Processing Steps . . . . .	23
<b>6 Implementation Results and Quantitative Comparison based on some Image Quality Metrics</b>	<b>24</b>
6.1 Image Quality metrics used: . . . . .	24

6.2	Implementation Results . . . . .	25
6.3	Evidence of Halo effect resolution . . . . .	28
6.4	Metric Results and Quantitative Comparison . . . . .	29
6.4.1	PSNR . . . . .	29
6.4.2	UQI . . . . .	30
6.4.3	SSIM . . . . .	31
6.4.4	BRISQUE . . . . .	32
6.4.5	Observations and Insights . . . . .	33
<b>7</b>	<b>Conclusion</b>	<b>34</b>
<b>8</b>	<b>Scope for Future Work</b>	<b>35</b>
<b>References</b>		<b>36</b>

## List of Figures

Figure 2.1	Flow of Literature Review . . . . .	2
Figure 2.2	Flow of Implementation . . . . .	3
Figure 3.8	Image enhancement stages proposed by Fu et al. [1] . . . . .	15
Figure 4	Image enhancement stages proposed . . . . .	19
Figure 5.2	Halo effect . . . . .	22
Figure 6.3	Edge detection results to show reduction in the halo effect . . . . .	28
Figure 8	Unnatural output for blue images . . . . .	35

## **List of Tables**

Table 6.2(a)      Implementation Results . . . . .	26
Table 6.2(b)      Implementation Results (cont'd) . . . . .	27
Table 6.4.1(a) . . . . .	29
Table 6.4.1(b) . . . . .	29
Table 6.4.2(a) . . . . .	30
Table 6.4.2(b) . . . . .	30
Table 6.4.3(a) . . . . .	31
Table 6.4.3(b) . . . . .	31
Table 6.4.4(a) . . . . .	32
Table 6.4.4(b) . . . . .	32



# 1 Introduction

Underwater images are of paramount importance in underwater scientific missions aimed at monitoring sea life and assessing the geological or biological environment. They are also used for the development and utilisation of deep-sea resources.

This brings us to the question, “*Why do we need to process these underwater images?*”.

To answer this, we need to examine the Light absorption and scattering problem. It is the chief reason for degradation of the quality of underwater images. It is known to cause problems in captured images like colour distortion, contrast reduction, fuzziness/haziness, underexposure and so on.

*The Light Absorption and Scattering problem:* The marine environment has suspended particles which absorb light and then re-emit it, thus scattering it. This process leads to attenuation of light as it goes deeper and deeper. It is important to note that different wavelengths of light get absorbed by the medium differently. The red colour is absorbed first owing to its high wavelength whereas the green and blue colours are not absorbed as much. Consequently, the green and/or blue colour predominate and the same is observed in all images captured under water. This is called colour cast and is a recurrent type of colour distortion.

The particles in the marine environment also reflect light back to the camera which interferes with the object’s reflected light. This is a key reason for the fuzziness and the poor contrast observed in underwater images. Many distant images are blurred in consequence. Furthermore, attenuation of underwater brightness is known to cause underexposure which is another issue having an adverse impact on the quality of underwater images.

Artificial light can be used to illuminate the scene. However, it is susceptible to light absorption and scattering as well, and hence, does not result in uniform lighting. Backscattering of light is another ill-effect of this, which leads to bright spots at the centre of the images and poor lighting at the periphery, which is not a desirable effect.

Thus, to overcome the aforementioned limitations, underwater image enhancement methods including underwater image dehazing algorithms, contrast enhancement algorithms are devised to improve specific image characteristics like colour, contrast and brightness.

Over the course of the project, we shall be exploring the Retinex model and the impact that incorporation of the bright channel prior and underwater dark channel prior algorithms have on the quality of an underwater image.



## 2 Project Flow

### 2.1 Flow of Literature Review

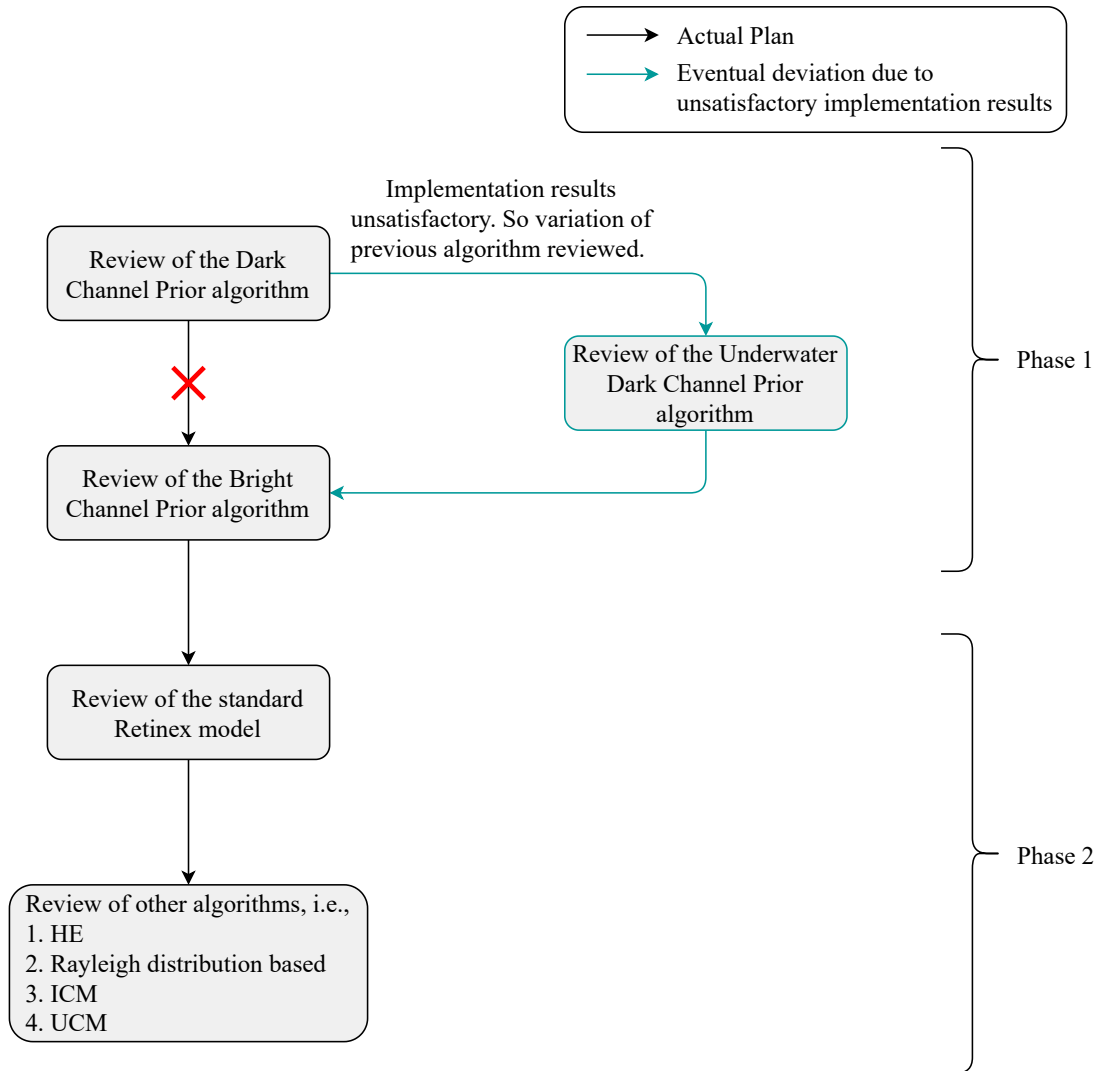


Figure 2.1: Flow of Literature Review



## 2.2 Flow of Implementation

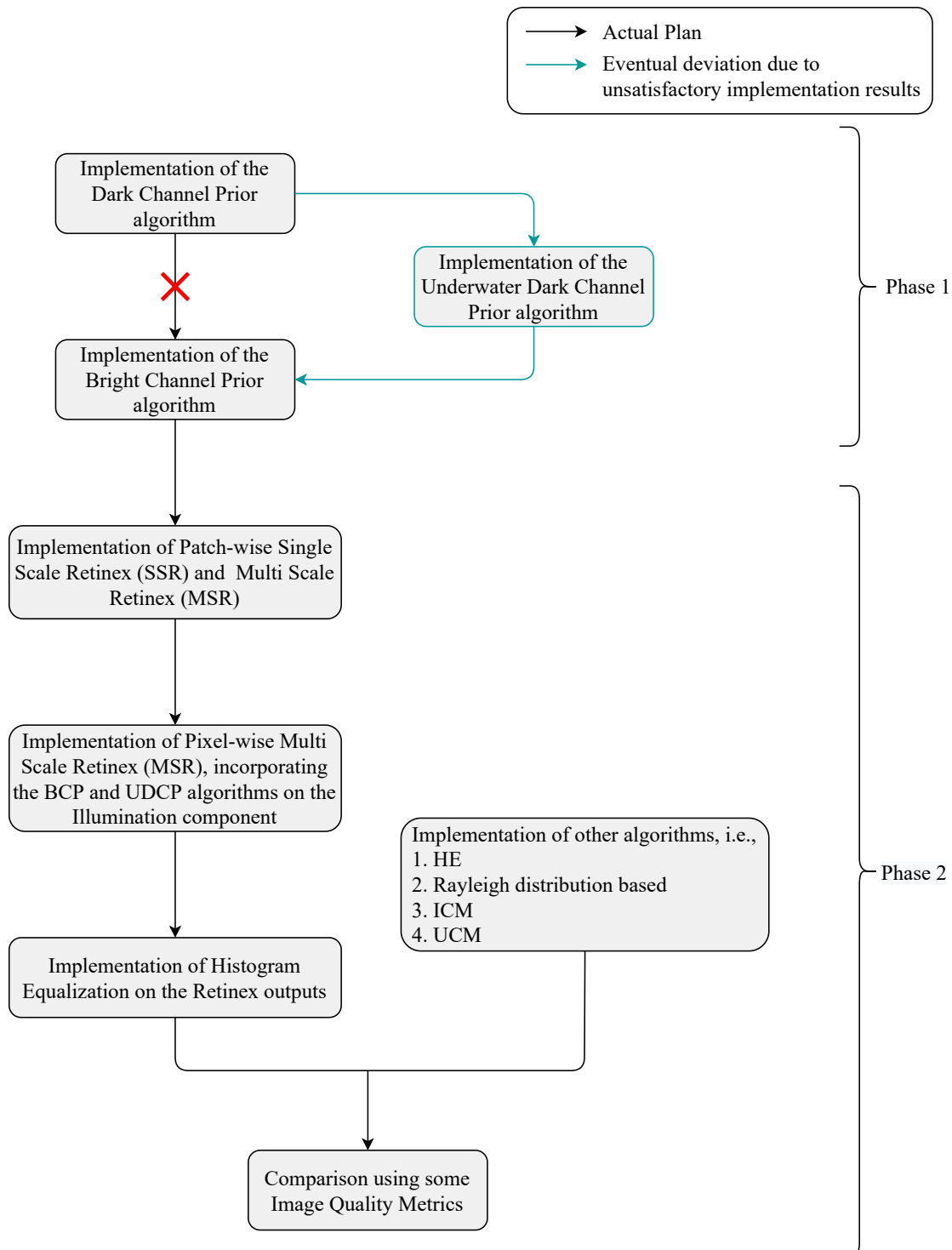


Figure 2.2: Flow of Implementation



### 3 Literature Survey

#### 3.1 The General Dark Channel Prior Algorithm

The General Dark Channel Prior algorithm is an image dehazing algorithm taking a hazy image input  $I$ . Marques et al. [2] mathematically modelled this image as shown:

$$I(x) = J(x)t(x) + A(1 - t(x)) \quad (1)$$

$$t(x) = e^{-\beta d(x)}$$

Here,  $I$  is the observed intensity (i.e., the input hazy image) whereas the dehazed image is represented by  $J$  (scene radiance).  $t$  is the transmission map which depicts the light reaching the camera without getting scattered or absorbed,  $A$  represents atmospheric light,  $\beta$  is the scattering coefficient of the atmosphere\* and  $d$  is the scene depth\*.

Our objective here is to find  $J$  by quantitatively determining  $A$  and  $t$  for the given input image  $I$ . There are four steps involved in this process:

1. *Finding the dark channel:* The dehazing process starts with the calculation of the dark channel.  $\Omega$  is a square patch centred at pixel  $x$  and having a fixed size. For such a patch, the dark channel is an image, composed of the pixel with the lowest intensity in that patch, factoring in all the channels. Marques et al. [2] presents the dark channel prior (DCP) as hinged on the assumption that the intensity of at least one pixel in one of the three colour channels of underwater images will be very less, i.e.,  $J^{dark}$  will tend to 0. This is supported by He et al. [3] who proved that a large majority of pixels in the dark channel have zero intensity, thus backing the dark channel prior assumption. Therefore,

$$J^{dark}(x) = \min_{y \in \Omega(x)} (\min_{c \in \{r,g,b\}} J^c(y)) \rightarrow 0 \quad (2)$$

2. *Finding atmospheric light A:*  $A$  is deemed as the most haze-opaque region in the image. It can be determined by first choosing the 0.1% brightest pixels in the dark channel.

---

\*Not pertinent to our study; ergo, we do not consider it.



The next step can be carried out in two ways, either by evaluating the mean of these 0.1% brightest pixels, or by directly considering the intensities of the red, blue and green channels associated with the brightest pixel, as the atmospheric light  $A$ .

After finding  $A$ , we normalize eq. 1 with  $A$ . This is done independently for each channel  $c \in \{r, g, b\}$  as shown:

$$\frac{I^c(x)}{A^c} = t(x) \frac{J^c(x)}{A^c} + 1 - t(x) \quad (3)$$

3. *Finding the transmission map  $t(x)$ :* To obtain transmission map, we consider the normalized hazy image equation 3 where we apply the minimisation operator and then put  $J = 0$  in accordance with the principle of dark channel prior. The algorithm assumes the transmission in a patch as constant and hence  $t$  is independent of the minimisation operator as shown below:

$$\min_{y \in \Omega(x)} \left( \min_c \frac{I^c(y)}{A^c} \right) = t(x) \min_{y \in \Omega(x)} \left( \min_c \frac{J^c(y)}{A^c} \right) + 1 - t(x) \quad (4)$$

Here,  $A^c$  is the atmospheric light in each colour channel and its value ranges from 0 to 1. Also, the coefficient of  $t(x)$  is equal to 0 (from eq. 2,  $\min_{y \in \Omega(x)} (\min_{c \in \{r, g, b\}} J^c(y)) \rightarrow 0$  and  $A^c$  is always positive). Substituting and rearranging the terms, the expression for the transmission map  $t(x)$  turns out to be

$$t(x) = 1 - \omega \min_{y \in \Omega(x)} \left( \min_c \frac{I^c(y)}{A^c} \right) \text{ where } \omega \in (0, 1) \text{ and } A^c \in [0, 1]$$

At this stage, He et al. [3] considered the haze observed in images; which happens to be a fundamental problem in images having faraway objects. This haze is attributed to the suspended particles in the medium. This haze should be removed so that we can get relatively clearer images. However, there is one problem. It involves a phenomenon called *aerial perspective* which expounds that the haze present in images is instrumental in depth perception. Complete removal of haze may cause the image to seem unrealistic along with a loss of depth perception.

Therefore, we retain a variable amount of haze for the sake of perceiving faraway objects. This is done by including a constant parameter  $\omega$  ( $0 < \omega < 1$ ). The value of  $\omega$  is based on respective use-cases and we adaptively preserve more haze for more



faraway objects. By doing so, we can expect more realistic images after the dehazing process.

4. *Recovery of Scene Radiance:* The last step is to recover the scene radiance which is essentially the haze-less image. It involves using the obtained transmission map and atmospheric light to get  $J$  as shown in this equation. The recovered scene radiance is susceptible to noise where the denominator in the expression comes close to zero. Therefore, we define a lower bound  $t_0$  to the transmission map  $t(x)$ , i.e., we preserve a small amount of haze in very haze-dense regions. This is akin to what is being done by the parameter  $\omega$ .

The expression for scene radiance  $J(x)$  (obtained from rearranging eq. 1) is as follows:

$$J(x) = \frac{I(x) - A}{\max(t(x), t_0)} + A$$

Upon recovery of scene radiance, we observe a shortcoming in the recovered image, which is the presence of blocking artifacts and halos. This is because our assumption that the transmission is always constant in a patch is not always true. Therefore, this is a downside of this algorithm.

## 3.2 Underwater Dark Channel Prior Algorithm

The Underwater Dark Channel Prior algorithm is modelled as a special case of the general dark channel prior algorithm but yields better results for underwater images when compared to the general algorithm. The difference lies in the fact that for the underwater dark channel prior, we make use of only the green and blue channels in our computation. On the other hand, as stated before, all three channels are involved in the general algorithm.

Now comes the main question: “*Why should we incorporate this? Isn’t the general algorithm good enough?*” Drews-Jr et al. [4] quote two reasons for this. Firstly, it is difficult to model red channel behaviour when it comes to underwater images. As mentioned in the introduction, with depth, the medium absorbs different wavelengths differently. Red is absorbed the most, resulting in a dominance of the green and/or blue colour (colour cast) in the underwater imagery. As a result, many pixels in the red channel have an intensity close to zero which makes the channel difficult to handle. This is largely observed in images having shadows, or underwater objects like fishes, algae, corals or rocks.



The second reason for omission of the red channel is a consequence of the first stated reason. It has been seen experimentally that the transmission estimate gets corrupted because of the many pixels being dark in the red channel. This causes the general dark channel prior algorithm to fail when restoring most underwater images.

*Quantitative treatment of the algorithm:* Drews-Jr et al. [4] model the image in the same way as the general dark channel prior algorithm, i.e.,

$$I(x) = J(x)t(x) + A(1 - t(x))$$

However, the expression of  $J^{dark}(x)$  in the case of UDCP takes into consideration only the green and blue channels as shown:

$$J^{dark}(x) = \min_{y \in \Omega(x)} (\min_{c \in \{g,b\}} J^c(y)) \rightarrow 0$$

To find the atmospheric light  $A$ , we select the intensity of the brightest pixel in each of the two channels as the atmospheric light. Next, the transmission map is obtained by substituting the value of  $J$  ( $= 0$ ) in the normalized image equation, like in the case of the general dark channel prior algorithm. The expression for scene radiance also remains the same but with  $c$  only composed of the green and blue channel. Also similar to the general algorithm is the presence of the parameters  $\omega$  and  $t_0$  which intend to preserve some haze so that we can obtain realistic images.

$$t(x) = 1 - \omega \min_{y \in \Omega(x)} \left( \min_c \frac{I^c(y)}{A^c} \right) \text{ where } \omega \in (0, 1) \text{ and } A^c \in [0, 1]$$

$$J(x) = \frac{I(x) - A}{\max(t(x), t_0)} + A$$

### 3.3 The Bright Channel Prior Algorithm

Sun and Xuo [5] used the same model as the one employed for the dark channel prior to characterize the hazy image as shown:

$$I(x) = J(x)t(x) + A(1 - t(x)) \quad (5)$$



$$t(x) = e^{-\beta d(x)}$$

The variables shown have the same meaning as the ones mentioned before. Following are the steps stipulated by the algorithm to find  $J$ :

1. *Finding the bright channel:* For a square patch  $\Omega$  of a given size in the hazy input image, the bright channel is an image, consisting of the pixel having the highest value of intensity in that patch. This is done considering all three colour channels. Thus, the bright channel is represented as

$$J^{bright}(x) = \max_{y \in \Omega(x)} (\max_{c \in \{r,g,b\}} J^c(y)) \quad (6)$$

2. *Finding atmospheric light A:* This is calculated in a fashion similar to that of the dark channel prior but the main difference is that we choose the pixel with the lowest intensity or we consider the mean of a group of pixels with lowest intensities (instead of highest) to find  $A$ .

After calculating  $A$ , we normalize eq. 5 with  $A$  for all  $c \in \{r, g, b\}$  as shown (calculations for each channel done independently):

$$\frac{I^c(x)}{A^c} = t(x) \frac{J^c(x)}{A^c} + 1 - t(x) \quad (7)$$

3. *Finding the transmission map  $t(x)$ :* We now apply maximisation operator on both sides of eq. 7. Akin to what is done in the dark channel prior algorithm, the transmission is assumed to be constant in a local patch  $\Omega(x)$  and hence is independent of the maximisation operator as shown:

$$\max_{y \in \Omega(x)} \left( \max_c \frac{I^c(y)}{A^c} \right) = t(x) \max_{y \in \Omega(x)} \left( \max_c \frac{J^c(y)}{A^c} \right) + 1 - t(x) \quad (8)$$

Upon rearrangement of eq. 8, we get the expression for transmission map  $t(x)$  as follows:

$$t(x) = \frac{\max_{y \in \Omega(x)} (\max_c I^c(y)) - A^c}{\max_{y \in \Omega(x)} (\max_c J^c(y)) + M - A^c}$$

Here,  $M$  is an optional brightness parameter which is adjusted according to the requirement of applications.



4. *Recovery of Scene Radiance*: The scene radiance can be procured from the computed atmospheric light and transmission map as shown in the following equation:

$$J(x) = \frac{I(x) - A}{\max(t(x), t_0)} + A$$

$t_0$ , is a constant aimed at limiting the lowest value of the denominator. This is for preservation of some haze.

### 3.4 Histogram Equalization

With the objective of equalizing pixel intensity values of the image, Ghani and Isa [6] employed the technique of Histogram Equalization (HE) where they “stretched” the histogram of each image channel over the complete dynamic range, that is, [0, 255]. The resulting stretched histogram of every colour channel embodied a better distribution of pixels. The equation used for this stretching process is:

$$I_{out} = (I_{in} - lv_i) \left( \frac{hv_o - lv_o}{hv_i - lv_i} \right) + lv_o$$

Here,  $I_{in}$  is the intensity of the pixel under consideration, i.e., the input pixel.  $I_{out}$  is the resultant intensity of the pixel.

$lv$  represents the lowest intensity whereas  $hv$  represents the highest intensity of the image. Subscripts  $o$  and  $i$  correspond to the output image and the input image respectively.

On account of the dynamic range being [0, 255],  $lv_o$  and  $hv_o$  can be substituted with 0 and 255, respectively. In doing so, the equation obtained is:

$$I_{out} = 255 \times \left( \frac{I_{in} - lv_i}{hv_i - lv_i} \right) \quad (9)$$

Now, we arrive at the inevitable question - “*What purpose does Histogram Equalization serve?*”. Histogram Equalization leads to uniform utilisation of the full range of intensities in the histogram, as stated above. Further, it can be observed that image contrast is mostly degraded because of some intensities that occur frequently in images. Histogram Equalization can alleviate this degradation by evenly spreading out these frequently occurring intensities, thus stretching the intensity range of images. This process causes regions with lower contrast to acquire a higher contrast, thereby increasing the global contrast of images.



### 3.5 Rayleigh Distribution based enhancement

Ghani and Isa [6] proposed a method of image enhancement based on the Rayleigh distribution. This technique involves histogram equalization which has been dealt with in the previous section. The technique proposed is described in the following series of steps:

1. The histogram of intensity values of the images is subjected to global stretching. In other words, histogram equalization is the first step in the Rayleigh-stretching process as mentioned above.
2. The average pixel intensity value is calculated for each channel using a technique suggested by Iqbal et al. [7] and Barnard et al. [8]. It is as shown:

$$R_{average} = \frac{1}{M \times N} \sum_{i=1}^M \sum_{j=1}^N I_R(i, j)$$

$$G_{average} = \frac{1}{M \times N} \sum_{i=1}^M \sum_{j=1}^N I_G(i, j)$$

$$B_{average} = \frac{1}{M \times N} \sum_{i=1}^M \sum_{j=1}^N I_B(i, j)$$

$M \times N$  represents the number of pixels in each channel.  $I_X(i, j)$  is the intensity of the pixel at position  $(i, j)$  of the  $X$  channel where  $X \in \{R, G, B\}$ .

3. Based on this average value, the histogram obtained in step 1 for each channel is divided into two regions - the lower and the upper region. The lower region comprises an intensity range of 0 to the computed average value. On the other hand, in the upper region, the intensity ranges from the average value to 255.
4. *Independent Stretching of the two regions:* The two regions of the histogram are subjected to stretching, where each histogram is stretched independently. This produces two separate histograms. This stretching is done based on the Rayleigh distribution whose probability distribution is

$$PDF_{Rayleigh} = \left( \frac{x}{\theta^2} \right) e^{\left( \frac{-x^2}{2\theta^2} \right)} \text{ for } x \geq 0, \theta > 0$$

where  $\theta$  is the distribution parameter of Rayleigh distribution and  $x$  is the input data.



This input is actually the intensity value obtained in step 1. Substituting  $x$  with  $I_{out}$  from eq. 9, the equation for Rayleigh-based stretching is obtained. Hence, the Rayleigh-stretched distribution is depicted as:

$$\text{Rayleigh - stretched} = \frac{255}{\theta^2} \left( \frac{I_{in} - lv_i}{hv_i - lv_i} \right) e^{-\frac{[255(I_{in} - lv_i)]^2}{2\theta^2(hv_i - lv_i)^2}}$$

Note that for the lower region,  $hv_i$  is the computed average intensity value and  $lv_i$  is the lowest intensity value in the region. For the upper region,  $hv_i$  is the highest intensity value in the region and  $lv_i$  is the average intensity value.

The lower region which used to lie between 0 and the average value will be stretched to the entire dynamic range of [0, 255]. Similarly, the upper region which used to lie from the average value to 255 is now stretched to the whole dynamic range of [0, 255]. Therefore, in both cases,  $lv_o$  and  $hv_o$  are 0 and 255 respectively (same as what has been done in the previous section).

5. Finally, the two resulting histograms are then composed, that is to say, combined to generate the enhanced image.

### 3.6 Integrated Colour Model

Iqbal et al. [9] proposed a way to combat the light absorption and scattering phenomenon in the undersea environment and also to mitigate the lighting/illumination problem (discussed in the Introduction). This technique, known as Integrated Colour Model (ICM) is based on the approach of slide stretching, which is composed of the following steps:

1. *Contrast stretching of RGB image*: Done using histogram equalization, this step intends to bring about uniform colour contrast in the image. The red and green channels of the image are balanced in such a way that they match or are somewhat similar to the blue channel of the given image. The obvious result is a more spread-out histogram and an image with a higher contrast. It goes without saying that each channel is subjected to stretching with the same scaling so that the correct colour ratio is maintained.
2. *Transformation of the RGB image to HSI*: The RGB image is converted into HSI (Hue, Saturation, Intensity) which provides a colour range that is wider. This wide colour range is provided by the Intensity (I) and Saturation (S) components (Hue describes



the pure colour of the image and Saturation depicts the extent up to which white light is mixed with the pure colour/hue of the image). Varying these components gives us leeway to control the contrast ratio of the underwater image. Hence, the true colour of images and their brightness can be increased as necessary.

3. Ultimately, the true colour of the underwater images can be procured by means of the Saturation component whereas the Intensity component accounts for the lighting problem.

### 3.7 Unsupervised Colour Correction Method

As mentioned before, underwater images are subject to colour distortion due to variable absorption and scattering of light under water. In an attempt to remedy this, Iqbal et al. [7] devised an Unsupervised Colour Correction Method (UCM). This was targeted at images that are predominantly green or blue (i.e., images with colour cast). This method has been observed to resolve colour cast as well as enhance the red component, the true colour and the illumination of the image, thus resulting in superior images. The steps involved in this process can be expounded as follows:

1. *RGB colour channel equalization*: This is done because there is little to no colour balance in underwater images because of blue/green colour cast. Normalizing the colour helps in rectifying this problem. The most prominent colour channel is considered the target and the remaining colours are increased up to the level of the target, thus bringing out a balance among all colours.
2. *Contrast correction of RGB image*: Contrast correction is done to improve the contrast in images. On a more fundamental level, stretching of the histogram is the process being performed.

The histogram can be stretched in three ways based on the occurrence of each colour component in the image:

- (a) To the upper side: This aims to select the lowest colour component of the image which is generally the red colour and is stretched towards the maximum side.
- (b) To the lower side: this aims to pick the prominent colour component of the image and decrease or stretch it towards the minimum side



- (c) To both sides: This aims to choose the median colour component and stretch it towards both, the minimum and maximum sides.
3. *Contrast correction of HSI colour model:* This step is same as the one undertaken in the Integrated Colour Model. The RGB image is converted to HSI. Next, the Saturation and Intensity components are changed as necessary. Upon completion of this process, the true colour of the underwater images is derived from the saturation component and illumination from the intensity component.

The selling point of UCM method is that it effectively enhances an image based on that image's properties and not based on static criteria.

## 3.8 The Retinex model

*Retinex – “Retina” + “Cortex”*

Land et al. [10] exemplified the unusual nature of the human visual system and enunciated that the more widely-used colour vision theory cannot explain it. They postulated the Retinex theory which states that the human visual system is an efficient information stabilizer that can extract constant information from a scene irrespective of the lighting conditions. This is called the colour constancy mechanism of the human visual system. In addition to this, Lenka and Khandual [11] state that the attempt by Land et al. [10] was the earliest one to describe the colour perception of the human visual system. Since then, the Retinex theory has been used to drive various algorithms which aim to better the contrast of images with large dynamic range. As Retinex aligns with the human visual system, it is considered as a human-perception based image enhancement mechanism based on the method of illumination compensation. Retinex based algorithms provides colour constancy as well as dynamic range compression.

These colour constancy based techniques alter the RGB intensity values at each pixel and provide a good estimate of the colour information present in an image, without requiring prior information about illumination. As a result, these Retinex-based algorithms improve the visual rendition of images when lighting conditions are bad. To sum up, Retinex attempts to balance machine and human vision, and ensure colour constancy at the same time.

An image scene in a human being's eyes can be modelled as the product of its illumina-



tion and reflectance. Let  $I(x, y)$  represent the intensity of a pixel in the image  $I$ . Then,

$$I(x, y) = R(x, y) \times L(x, y)$$

Tang et al. [12] make use of this model of the image to explain the Retinex model. The basic idea here is to employ various ways to extract the illumination component. Reflectance is obtained by the subtraction of the illumination from the original image. Finally, after appropriate enhancement, combination of the transformed illumination and reflectance components gives us the final enhanced image. As a result, the naturalness of the enhanced images is preserved whereas other details can be enhanced. Retinex algorithms can be categorized into centre/surround based, recursive and path-based algorithms.

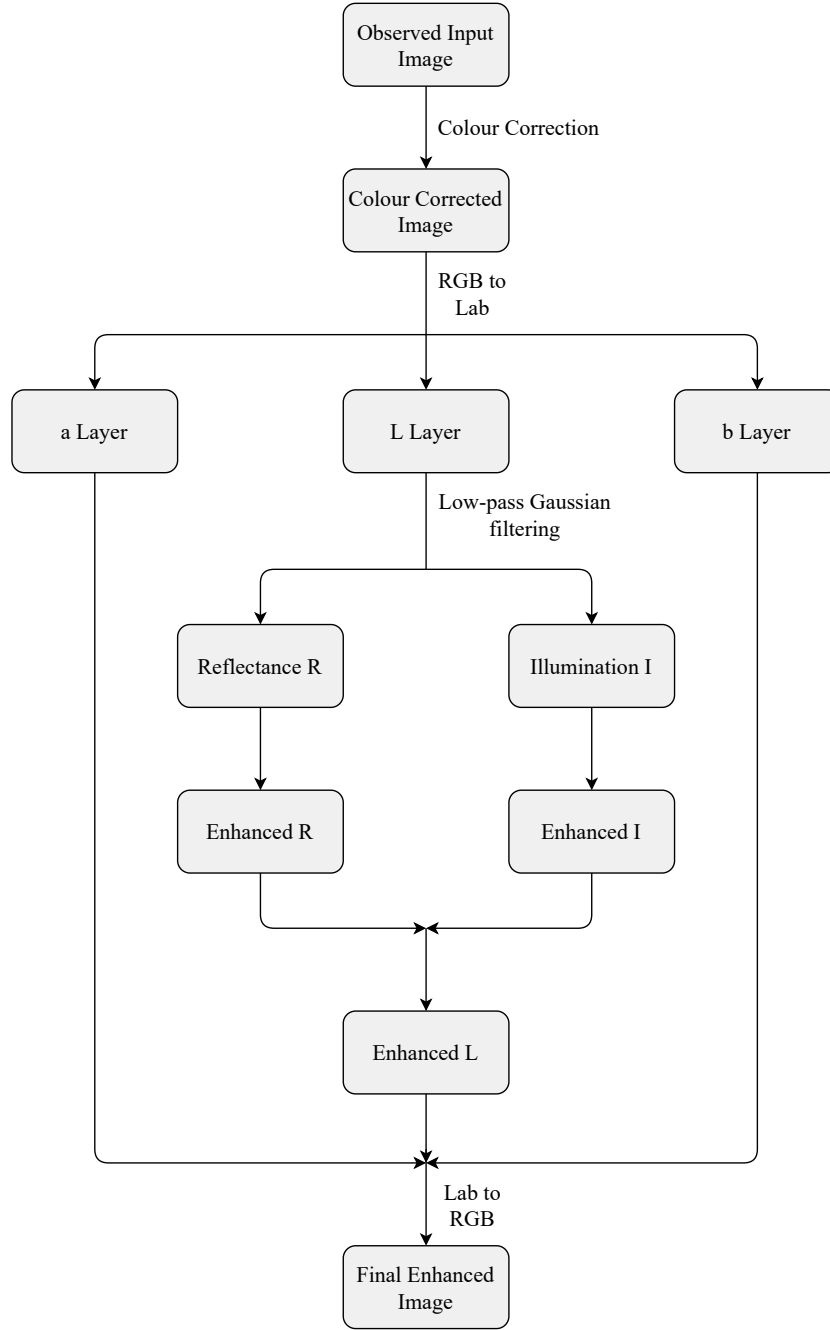


Figure 3.8: Image enhancement stages proposed by Fu et al. [1]

### 3.8.1 The Single Scale Retinex

The single scale Retinex is a centre/surround based Retinex algorithm. As previously introduced, the Retinex model regards an image  $I$  as the product of  $R(x, y)$  and  $L(x, y)$ . For each pixel  $(x, y)$ ,  $L(x, y)$  represents its illumination and  $L \in [0, 255]$  whereas  $R(x, y)$  represents its reflectance and  $R \in [0, 1]$ . Note that  $I$  varies from 0 to 255. Lenka and Khandual [11] explain that  $L(x, y)$  is based on the characteristic nature of the illumination source, whereas  $R(x, y)$  can be found from the imaged objects' characteristics. The following con-



straints/assumptions are also to be made when evaluating an image using this model –

1. The illumination of the image should be spatially smooth.
2.  $R$  varies from 0 to 1, which implies that  $L$  is always greater than or equal to  $I$ .
3. The reflectance is a high frequency component, i.e., texture and edge related information. On the other hand, the illumination component is a low frequency component.

Since the illumination is a low frequency component, a low-pass filter can be employed to extract it. SSR is a centre/surround based Retinex technique. It makes use of a logarithmic photoreceptor function in order to approximate/emulate the human visual system. Reflectance is obtained through the single scale Retinex using the following:

$$R(x, y) = \log I(x, y) - \log[F(x, y) * I(x, y)] \quad (10)$$

where  $F$  represents the surround space function. It is a function that calculates the average of neighbouring pixel values and allocates it to the pixel at the centre. The choice of surround space function influences the amount of dynamic range compression produced. Using surround functions like the Gaussian and the exponential result in good dynamic range compression. In our case, we used a Gaussian surround space function/Gaussian blur function, which goes as follows:

$$F(x, y) = \frac{1}{2\pi\sigma^2} e^{-\frac{x^2+y^2}{2\sigma^2}}$$

Some of the features of SSR are highlighted by Lenka and Khandual [11] and are as follows:

1. As depicted by eq. 10, log transformation/placement is performed subsequent to incorporation of the surround function.
2. Violation of the grey world assumptions leads to greying out of images, either locally or globally or in rare cases, colour distortion of images.

Rahman et al. [13] exhibit the existence of a trade-off between the extent of dynamic range compression and the colour/tonal rendition, which is to say, SSR is not capable of concomitantly imparting appreciable dynamic range compression as well as decent colour rendition. Due to this trade-off, only one factor can be improved, which is done at the cost of the



other. Adding to this, some detail loss also occurs because the surround space function (Gaussian filter) which is used causes image blurring. To remedy these problems, the multi scale Retinex was postulated.

### 3.8.2 The Multi Scale Retinex

In the hope of preserving both dynamic range compression and colour rendition of an image, the multi scale Retinex (MSR) was introduced. Lenka and Khandual [11] - The multi scale Retinex is represented as a weighted summation of a certain number of scales of the single scale Retinex. It is also computationally fast because the different samples are processed in a parallel manner. This technique is aimed at achieving gamma correction, dynamic range compression, colour constancy processing and colour enhancement.

MSR is mathematically defined as shown:

$$R_{MSR} = \sum_{n=1}^N \omega_n R_n$$

or

$$R_{MSR} = \sum_{n=1}^N \omega_n \{ \log I(x, y) - \log [F_n(x, y) * I(x, y)] \}$$

where  $R_n$  represents the reflectance component associated with the  $n^{th}$  scale,  $\omega_n$  represents the weight of the  $n^{th}$  scale and  $N$  is the chosen number of scales.  $F$  is the Gaussian surround space function, and it holds the same definition as used in the single-scale Retinex, i.e.,

$$F(x, y) = \frac{1}{2\pi\sigma^2} e^{-\frac{x^2+y^2}{2\sigma^2}}$$

Lenka and Khandual [11] and Rahman et al. [13] explain that the essence of the multi scale Retinex lies in the weights used and the number of scales needed.

The multi scale Retinex combines several weightings of the single scale Retinex, selects the right number of scales and also finds scales which can potentially be merged. It has been observed that three scales suffice for most images. Next, the best weights are chosen such that maximum dynamic range compression as well as colour/tonal rendition can be obtained. However, the weights can be fine-tuned to incline more towards dynamic range compression or towards color/tonal rendition or maintain a balance between the two. Usu-



ally, equal weights gives creditable results. Therefore, tailoring of parameters according to our requirements is what makes this technique attractive.

Images enhanced through MSR have substantial amount of dynamic range compression at the edges separating dark and light parts and decent colour/tonal rendition in the entire image scale. Thus, MSR accounts for illumination differences in order to emulate what humans perceive in a scene.

The surround space function in MSR is the same as that of SSR, i.e., the Gaussian surround function. Also, logarithmic transformation is applied after the surround space function evaluation, similar to what has been done in the case of SSR.

MSR is observed to preserve most of the detail in the scene. Therefore, the multi scale Retinex produces a much better final enhanced image when considering colour and dynamic range compression, when compared to the single scale Retinex.

However, even in the multi scale Retinex, it is hard to judge the fidelity of the reproduction of colour. Consequently, there may be some issues pertaining to colour sensitivity. Also, images enhanced by means of MSR still suffer from greying-out of uniform zones and hence, the overall result of enhancement through MSR is still more saturated than human observation. This gives the final image a washed-out appearance. These are some of the wrinkles in the multi scale Retinex that need to be ironed out.

As a whole, the multi scale Retinex is a very propitious method for underwater image enhancement. Research is always being conducted to incorporate other transmission-map based, histogram-based and variational-optimization based approaches in conjunction with Retinex models to get better enhancement of images. We aim at incorporating transmission-map based approaches (prior-based algorithms) in a Retinex model.



## 4 Flow of the Technique proposed

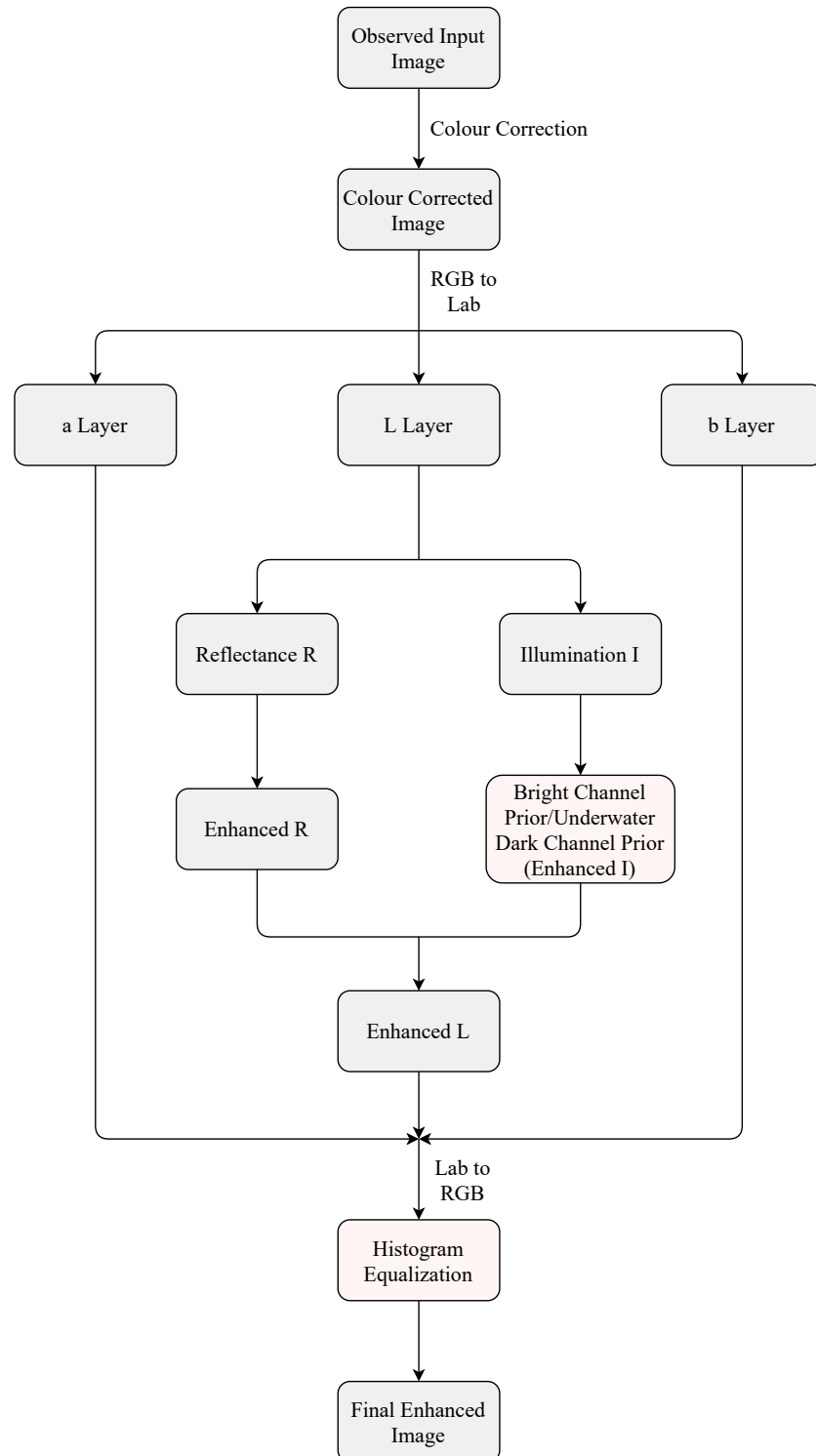


Figure 4: Image enhancement stages proposed



# 5 Working Principle

The working principle of our project is based on the Retinex-based model of image enhancement. Land and McCann [10] were the ones who proposed the Retinex theory and demonstrated that the human visual system (HVS) can deal with illumination that changes both brightness and colour adaptively. The Retinex methods enhance the input image by extracting the illumination component using low-pass filters and logarithmic transformation. However, a halo effect is observed near the edges. Fu et al. [14] proposed a BCP at the illumination to reduce said halo effects. We also find that the incorporation of UDCP at the same stage gives an output which is comparable or in some cases, even better than that of the BCP approach, depending on the image and its features.

The proposed method contains 3 major steps:

1. Pre-Processing Steps - Colour Correction and Conversion from RGB to Lab colour space
2. Incorporation of BCP/UDCP into the Retinex Algorithm
3. Post-Processing steps

## 5.1 Pre-Processing Steps

### 5.1.1 Colour Correction

Green and Blue lights have short wavelengths, to be specific, around 550 and 450 nm, respectively. Since these colours and their shades have short wavelengths, they travel the farthest in water and this is the reason for images taken under water appearing predominantly green or blue. Out of all the colours, red has the longest wavelength of about 700 nanometer and hence travels the least in water. It is safe to say that the colour red is almost non-existent in underwater images unless a close-up photo of a red object is taken.

Colour correction is an essential process in many fields where the light and the colours of an image are altered altogether. To address the colour cast, a colour correction technique based on a histogram equalization is being used. In histogram equalization, the contrast of each channel is enhanced, hence making the bright parts, brighter and the dark parts, darker.

The image is first divided into channels, which are red, green and blue. For every channel, the number of occurrences of each element in a flattened array is found, with values



spanning from 0 to 255. The number of occurrences of each element is stored at the corresponding index in an array. High and Low values are found from the above array. After this, new values are assigned to each level. If a level is lesser than the Low value ( $lv$ ), it is equated to zero and if it is greater than the High value ( $hv$ ), it is equated to 255. For levels that lie in between the Low and High values, they are equated to a normalized value (shown below).

This assignment of values is depicted in the below expression:

$$level = \begin{cases} 0 & \text{if } level < lv \\ \frac{(level-lv)}{(hv-lv)} \times 255 & \text{if } lv \leq level \leq hv \\ 255 & \text{if } level > hv \end{cases}$$

This is repeated for every channel and finally, to obtain the output image, all the three channels are merged.

### 5.1.2 Conversion of the RGB image to Lab

The CIE Lab colour space is a three-dimensional space which covers the whole range of human colour perception.

In order to convert RGB values to the Lab values, the reference illuminant of the RGB colour space and the RGB primary co-ordinates are stored in the form of a colour lookup table (CLUT), which is contained in most imaging and machine vision libraries and these are used to perform these conversions. While RGB operates on 3 channels, i.e., red, green and blue, Lab is a conversion of the same information to a brightness (luminosity) component L, and 2 colour components (channels) a and b.

Now comes the question – “*Why do we need to perform this conversion?*”. Justification for this can be provided by taking into account the benefits of the Lab colour space. Firstly, since one entire channel is dedicated to luminosity, it can be kept separate from the colour channels so that you can adjust one component without affecting the other. Secondly, the L component closely matches with the human visual system’s perception of lightness. Therefore, if we brighten an image or perform colour correction on an image in the CIE Lab colour space, the result will often look more accurate to the human visual system, colour wise. Thirdly, by using the CIE Lab colour space, we can shift colours, and pictures can be made more vibrant without changing the amount of saturation present in them. Also,



to-and-fro translations between RGB and Lab is lossless and this is very advantageous as information is not lost. Thus, Lab colour space relates better with human colour perception.

## 5.2 Implementation

The L layer, i.e., the Luminance layer of the obtained Lab image is taken and the Illumination and Reflectance components of the image are extracted from it, as shown in the flowchart. Illumination is piecewise smooth whereas the reflectance is piecewise constant and contains edges. In the Retinex model, the illumination component is found using low-pass Gaussian filters and the reflectance component is found by the subtraction of the illumination component from the original image. Howbeit, a halo effect at object edges may be observed which is undesirable. This is due to the illumination component of the image being continuous near object edges.

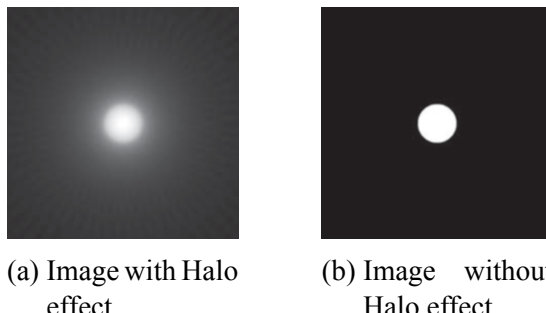


Figure 5.2: Halo effect  
Courtesy: Gonzalez and Woods [15]

To tackle this problem, we are using two approaches:

1. *BCP approach*: As mentioned above, the Retinex model based approach still suffers from a small halo effect because the illumination component is continuous near edges. To apply discontinuity, the bright channel prior algorithm is applied on the illumination component, which suppresses this halo effect. A pixel-wise bright channel is used to do this. This approach gives us the enhanced reflectance and illumination components of the image.
  2. *UDCP approach*: The UDCP algorithm, as mentioned previously, is specifically designed for underwater images where the red channel is not considered in the computation. This algorithm (applied pixel-wise in our case) has been proven to produce better images. The procedure is same as that of the BCP approach.



## 5.3 Post-Processing Steps

After obtaining the enhanced illumination and reflectance components, they are combined to get the L layer, i.e., the luminance layer. This, in turn, is merged with the a and b layers to get back the image in the Lab colour space. The image obtained is converted back to the RGB colour space to give an enhanced underwater image. Upon examination, the intensity of colour in the resultant image was found to be high, leading to loss of realism. We realized that applying Histogram Equalization to that image normalizes the intensity of colour in the image. The image obtained after applying Histogram Equalization is the final enhanced image.



# 6 Implementation Results and Quantitative Comparison based on some Image Quality Metrics

## 6.1 Image Quality metrics used:

There are two kinds of metrics to ascertain the quality of the obtained haze-less images. They are Full-Reference Quality Metrics and No-Reference Quality metrics and this classification is based on their requirement of another image as reference for predicting quality of images. We used three Full-Reference Quality Metrics and one No-Reference Quality Metric.

*Full-Reference Quality Metrics:*

1. PSNR (Peak Signal to Noise Ratio): As the name indicates, this metric is the ratio of the highest attainable power of a signal (of an image) to the power of the noise that corrupts that image. A high PSNR value indicates that the degree of enhancement achieved is low and vice versa. PSNR gauges the quality of the enhanced image based on only the reference image and not according to the human visual system; ergo, better evaluation metrics like UQI and SSIM are used.
2. UQI (Universal Image Quality Index): The Universal Image Quality index is a metric designed by Wang and Bovik [16]. This metric considers image distortion to be influenced by three aspects – contrast distortion, luminance distortion and loss of correlation. The metric is modelled mathematically without taking into account human perception. Even then, it is observed by means of experiments that the performance of UQI is much better than that of the more commonly seen PSNR metric. In the case of UQI, a higher score signifies that the amount of enhancement achieved is lower.
3. SSIM (Structural Similarity Index): SSIM is a metric that takes into account the brightness, contrast and structure of an image while gauging its quality. Therefore, it agrees more closely with the score as perceived by humans. The SSIM metric always gives a value between -1 and 1. A value closer to 1 depicts that the obtained image



has not been improved/enhanced much with respect to the initial image.

*No-Reference Quality Metric:*

1. BRISQUE (Blind/Referenceless Image Spatial Quality Evaluator): This metric does not require a reference images as it has been trained with a dataset of images having common and familiar distortions. Consequently, BRISQUE can only be used to assess the quality of images that are prey to the same or similar types of distortions. Along with the non-requirement of reference images, another merit of this metric is that it aligns well with human perception. The BRISQUE score ranges from 0 to 100 and lower values of the BRISQUE score reflect better perceptual quality of image.

## 6.2 Implementation Results

To evaluate the efficacy of the proposed technique for a large array of images, we employed ten images from the Underwater Image Enhancement Benchmark (UIEB) dataset constructed by Li et al. [17]. In addition to that, the same ten images were subjected to enhancement through the other reviewed algorithms so as to see how well the proposed method fares against traditional or pre-existing techniques. A visual representation of the results for three such images are given in the tables on the next couple of pages.

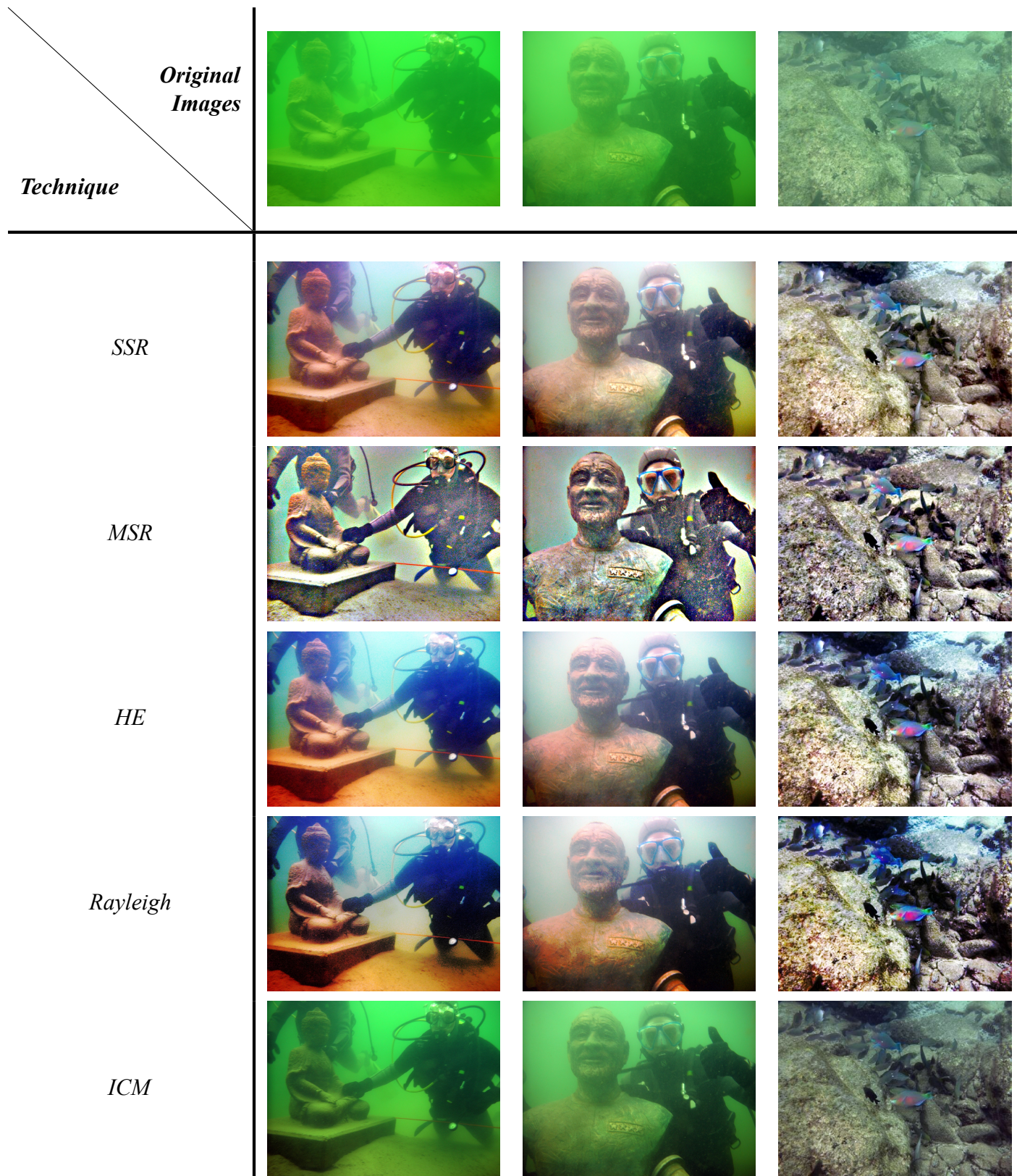


Table 6.2(a): Implementation Results



<i>Original Images</i>			
<i>Technique</i>			
<i>UCM</i>			
<i>MSR+ BCP</i>			
<i>MSR+ UDCP</i>			
<i>MSR+ BCP+ HE</i>			
<i>MSR+ UDCP+ HE</i>			

Table 6.2(b): Implementation Results (cont'd)



## 6.3 Evidence of Halo effect resolution

To prove that our technique has mitigated the halo effect problem, we have employed a general image processing technique called edge detection. We perform this using the Sobel filter. Gonzalez and Woods [15] stated that the halo effect covers the edges of the object as a result of which object edges are not well-defined. Obviously, object edges that are not well-defined cannot be detected by the Sobel filter. This fact is illustrated in Figure 6.3a where hardly any edges are visible. On the other hand, well-defined edges are visible in Figures 6.3b and 6.3c. This is a direct implication that the multi scale Retinex and consequently, our proposed method (with BCP) have alleviated the halo effect problem.

*Image considered:* Image 1 from implementation results (composed of a diver and a Buddha statue)

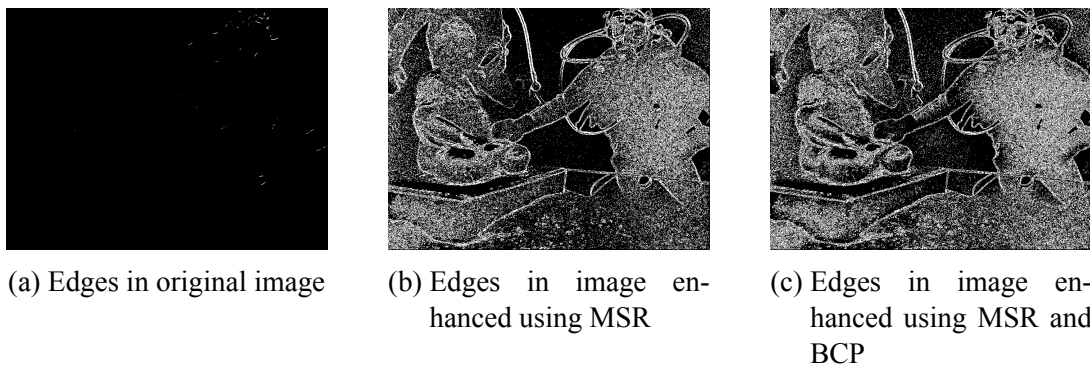


Figure 6.3: Edge detection results to show reduction in the halo effect



## 6.4 Metric Results and Quantitative Comparison

Efficacy of each algorithm/technique vis-à-vis a particular metric can be determined by means of the values of that metric for that algorithm.

Each algorithm is first implemented on all the ten images. Next, the four metrics are applied on each output. The results are as shown.

### 6.4.1 PSNR

Image	<i>ICM</i>	<i>UCM</i>	<i>Rayleigh</i>	<i>HE</i>	<i>SSR</i>	<i>MSR</i>
1	15.9663	12.7136	9.197	8.5424	8.9718	8.5648
2	18.6543	14.7806	10.9706	10.5309	10.5833	9.7926
3	15.8357	10.7189	11.8884	12.425	14.4227	12.2046
4	13.6953	13.9409	12.0715	12.0981	12.6855	12.2431
5	13.6753	10.8628	11.2051	11.9844	12.0627	11.4247
6	11.8648	11.8806	7.7921	7.3682	8.0057	7.6295
7	18.8652	21.3471	10.2232	9.2758	9.0128	9.4398
8	11.9934	10.1198	10.0443	9.9111	10.4119	9.3438
9	18.8419	14.7991	12.2585	10.8433	11.9781	10.1147
10	16.2096	13.2104	12.8327	13.3239	14.5341	13.8556

Table 6.4.1(a)

Image	<i>MSR + BCP</i>	<i>MSR + UDCP</i>	<i>MSR+BCP+HE</i>	<i>MSR+UDCP+HE</i>
1	9.1934	9.5137	8.0594	8.0371
2	10.2407	10.1705	8.9894	8.7851
3	12.0791	10.096	10.9958	10.8356
4	12.1032	11.5464	11.1485	11.1196
5	10.4257	10.0406	10.7057	10.6596
6	8.0539	8.484	7.3519	7.3599
7	10.1121	10.6016	9.0044	8.9853
8	8.8399	8.5098	9.0317	8.9838
9	10.8471	11.5299	9.5929	9.5702
10	13.1804	12.9136	12.2732	12.3088

Table 6.4.1(b)



#### 6.4.2 UQI

Image	<i>ICM</i>	<i>UCM</i>	<i>Rayleigh</i>	<i>HE</i>	<i>SSR</i>	<i>MSR</i>
1	0.891199	0.762520	0.566353	0.529737	0.499935	0.498147
2	0.918214	0.792083	0.678524	0.673682	0.656530	0.624306
3	0.802793	0.505763	0.614048	0.746213	0.797802	0.774220
4	0.692201	0.702383	0.684190	0.751849	0.808470	0.809158
5	0.804247	0.639055	0.666142	0.751994	0.764716	0.764521
6	0.552725	0.504874	0.363930	0.364204	0.395404	0.373152
7	0.842427	0.904398	0.583530	0.574418	0.547422	0.570959
8	0.706782	0.613816	0.650495	0.654839	0.659678	0.621162
9	0.845606	0.692184	0.675614	0.658799	0.697459	0.620775
10	0.862955	0.717818	0.749036	0.804728	0.865610	0.853623

Table 6.4.2(a)

Image	<i>MSR + BCP</i>	<i>MSR + UDCP</i>	<i>MSR+BCP+HE</i>	<i>MSR+UDCP+HE</i>
1	0.518090	0.539194	0.484430	0.485379
2	0.637269	0.621739	0.587129	0.576418
3	0.746523	0.588385	0.710103	0.695733
4	0.751478	0.692904	0.730601	0.733507
5	0.676936	0.636165	0.721189	0.719837
6	0.370425	0.377608	0.355635	0.355994
7	0.561328	0.546720	0.530271	0.520697
8	0.558840	0.524324	0.605134	0.604490
9	0.628697	0.631220	0.583207	0.584228
10	0.802841	0.774712	0.782237	0.782697

Table 6.4.2(b)



### 6.4.3 SSIM

Image	<i>ICM</i>	<i>UCM</i>	<i>Rayleigh</i>	<i>HE</i>	<i>SSR</i>	<i>MSR</i>
1	0.74878	0.49101	0.10108	0.085879	0.017244	0.091105
2	0.77025	0.52455	0.092366	0.065961	0.099874	0.090361
3	0.62015	-0.039956	0.17788	0.26668	0.44247	0.33965
4	0.48987	0.36653	0.26527	0.19498	0.32292	-0.034515
5	0.29756	-0.20852	0.046808	0.11696	-0.10933	0.092177
6	0.35568	0.42506	0.060694	0.061763	0.17306	0.13974
7	0.72065	0.8795	0.14641	0.078682	0.09809	0.095022
8	0.14499	-0.22486	0.064519	0.023279	0.19021	-0.12063
9	0.65923	0.23589	0.16153	0.12211	0.14563	0.13399
10	0.6076	0.27536	0.33985	0.36099	0.40065	0.30155

Table 6.4.3(a)

Image	<i>MSR + BCP</i>	<i>MSR + UDCP</i>	<i>MSR+BCP+HE</i>	<i>MSR+UDCP+HE</i>
1	0.12026	0.13893	0.03827	0.38297
2	0.12305	0.12982	0.035413	0.03718
3	0.37431	-0.059113	0.1599	0.075657
4	-0.066759	-0.078854	0.10358	0.10074
5	0.085549	0.077777	0.093554	0.091005
6	0.14436	0.1613	0.066338	0.068569
7	0.10227	0.1072	0.047329	0.050838
8	-0.13395	-0.14336	0.011341	0.010213
9	0.14594	0.14537	0.10928	0.12374
10	0.28263	0.27927	0.27027	0.27204

Table 6.4.3(b)



#### 6.4.4 BRISQUE

Image	<i>ICM</i>	<i>UCM</i>	<i>Rayleigh</i>	<i>HE</i>	<i>SSR</i>	<i>MSR</i>
1	28.9905	27.8655	30.8738	31.4082	31.9572	40.0024
2	29.8363	17.8036	24.8483	26.5064	20.3398	38.8194
3	32.2478	31.508	24.1867	29.5529	32.6125	28.8586
4	26.0417	28.9769	9.9352	7.565	16.5957	34.8151
5	32.6142	25.2204	17.77	21.672	21.1195	24.4136
6	44.9348	42.1639	38.017	38.8158	41.1114	32.9947
7	48.3751	39.5948	28.802	31.634	27.1235	33.0581
8	40.5906	27.674	16.289	14.2463	19.7944	29.58
9	39.4363	38.3288	29.838	35.8189	29.75	39.4199
10	34.0859	28.5576	17.255	14.5392	18.942	19.3171

Table 6.4.4(a)

Image	<i>MSR + BCP</i>	<i>MSR + UDCP</i>	<i>MSR+BCP+HE</i>	<i>MSR+UDCP+HE</i>
1	39.7587	39.0188	38.862	38.0139
2	38.77	38.0997	38.2744	37.0443
3	29.3958	30.2847	30.3409	36.6257
4	31.7395	29.4417	24.0871	22.4904
5	23.9003	22.3279	28.0628	27.7201
6	31.7435	31.468	32.1711	30.2844
7	33.9303	30.2747	34.9984	32.091
8	26.2763	25.4626	33.6962	33.1892
9	38.3589	34.24	27.4015	29.7515
10	18.2619	17.498	23.1037	22.2946

Table 6.4.4(b)



#### 6.4.5 Observations and Insights

The above table depicts average values of metrics performed on images enhanced by different techniques. For every image metric, lower the value, better the enhancement technique used. A few observations on the metric results are given below:

1. *Peak Signal to Noise Ratio (PSNR)*: PSNR presents the combination of MSR, UDCP and HE as the best solution. The combination of MSR, BCP and HE also performs reasonably well. The difference in performance between the two is because of UDCP being a component of the former, which gives an edge over BCP in the case of underwater images.
2. *Universal Image Quality Index (UQI)*: According to the results obtained through UQI, the combination of MSR and UDCP provide the best results. MSR + UDCP + HE and MSR + BCP + HE are not far behind in performance.
3. *Structural Similarity Index (SSIM)*: The SSIM metric is in agreement with the UQI metric with regard to the combination of MSR and UDCP being the best technique. Following closely behind is combination of MSR, BCP and HE. However, the metric results show that the MSR + UDCP + HE combination is not up to the mark. This implies that the results of this combination may not conform with the subjective score given by human perception of images.
4. *Blind/Referenceless Image Spatial Quality Evaluator (BRISQUE)*: According to BRISQUE, enhancement solely based on Rayleigh Distribution produces the best enhanced image. The proposed methods, i.e., MSR + BCP + HE and MSR + UDCP + HE yield slightly high values of BRISQUE metric. Nevertheless, the results are up to par.

Overall, It is evident that Retinex models involving UDCP generally perform better than the ones with BCP (with the exception of SSIM). This is obvious because the UDCP algorithm is tailor-made for underwater images. Also, the proposed methods are relatively successful in keeping detail loss to a minimum, when compared to the other pre-existing algorithms.



## 7 Conclusion

Owing to the light absorption and scattering problem, underwater images fall prey to fuzziness, contrast reduction, underexposure and colour cast. Our aim was to tackle all these problems by finding an effective technique to remedy this. Some pre-existing low-light image enhancement algorithms were surveyed before delving into the depths of novel image enhancement techniques.

The survey, as a part of Phase 1, comprised a review of different enhancement algorithms, i.e. the Dark Channel Prior, the Underwater Dark Channel Prior and Bright Channel Prior algorithms. Quantitative comparison was carried out by means of Image Quality Metrics like Peak Signal to Noise Ratio (PSNR), Universal Image Quality Index (UQI), Structural Similarity Index (SSIM) and Blind/Referenceless Image Spatial Quality Evaluator (BRISQUE). Satisfactory results were obtained for all algorithms except the DCP algorithm.

In Phase 2 of the project, we started with a review of the Retinex model where we looked at its single scale (SSR) and multi scale (MSR) variants. Implementation of the same was done as well. A review of four other pre-existing algorithms (i.e., Histogram Equalization, Rayleigh distribution based, Integrated Colour Model and Unsupervised Colour Correction method) was also done simultaneously, followed by implementation. The proposed methods, i.e., the combination of MSR and BCP and the combination of MSR and UDCP were implemented. The intensity of colour in the images obtained as output was very high, leading to some unrealism. We employed HE as a post-processing step to resolve this colour intensity issue. Lastly, as done in phase 1, the four metrics were used to quantify the efficacy of each of the algorithms. The proposed techniques fared pretty well and our objective of minimising detail loss during the course of enhancement was fulfilled. The only unsatisfactory result was the SSIM metric result for the combination of MSR, UDCP and HE, which suggested that the technique needs to improve to make it more pleasing to the human eye.



## 8 Scope for Future Work

As evident from the implementation results and conclusions, the problem of colour cast and halo effect has been resolved. The loss of detail during this enhancement process is also minimum. However, when it comes to human perception of images, the SSIM metric, which aligns with human perception depicts the combination of MSR, BCP and HE as unsatisfactory. This would imply that images generated by this method are not up to par when perceived by humans. Newer techniques can be devised where images are pleasing to the human eye as well as not subject to detail loss.

Another problem encountered during the course of research involved images with predominant blue colour. Enhancement of such images led to orange-red outputs which were highly unnatural. One such instance is shown:



(a) Original Image (b) Enhanced Image

Figure 8: Unnatural output for blue images

Therefore, the technique needs some fine-tuning to adapt to blue underwater images so that realistic images are obtained. This is another area where there is scope for improvement.



# References

- [1] X. Fu, P. Zhuang, Y. Huang, Y. Liao, X.-P. Zhang, and X. Ding, “A retinex-based enhancing approach for single underwater image,” in *2014 IEEE International Conference on Image Processing (ICIP)*, 2014, pp. 4572–4576.
- [2] T. P. Marques, A. B. Albu, and M. Hoeberechts, “Enhancement of low-lighting underwater images using dark channel prior and fast guided filters,” in *Pattern Recognition and Information Forensics*, Z. Zhang, D. Suter, Y. Tian, A. Branzan Albu, N. Sidère, and H. Jair Escalante, Eds. Cham: Springer International Publishing, 2019, pp. 55–65.
- [3] K. He, J. Sun, and X. Tang, “Single image haze removal using dark channel prior,” *IEEE Transactions on Pattern Analysis and Machine Intelligence*, vol. 33, no. 12, pp. 2341–2353, 2011.
- [4] P. Drews Jr, E. do Nascimento, F. Moraes, S. Botelho, and M. Campos, “Transmission estimation in underwater single images,” in *2013 IEEE International Conference on Computer Vision Workshops*, 2013, pp. 825–830.
- [5] S. Sun and X. Guo, “Image enhancement using bright channel prior,” in *2016 International Conference on Industrial Informatics - Computing Technology, Intelligent Technology, Industrial Information Integration (ICIICII)*, 2016, pp. 83–86.
- [6] A. S. A. Ghani and N. A. M. Isa, “Underwater image quality enhancement through composition of dual-intensity images and rayleigh-stretching,” in *2014 IEEE Fourth International Conference on Consumer Electronics Berlin (ICCE-Berlin)*, 2014, pp. 219–220.
- [7] K. Iqbal, M. Odetayo, A. James, R. A. Salam, and A. Z. H. Talib, “Enhancing the low quality images using unsupervised colour correction method,” in *2010 IEEE International Conference on Systems, Man and Cybernetics*, 2010, pp. 1703–1709.
- [8] K. Barnard, V. Cardei, and B. Funt, “A comparison of computational color constancy algorithms. i: Methodology and experiments with synthesized data,” *IEEE Transactions on Image Processing*, vol. 11, no. 9, pp. 972–984, 2002.



- [9] K. Iqbal, R. Abdul Salam, O. Azam, and A. Talib, "Underwater image enhancement using an integrated colour model," *IAENG International Journal of Computer Science*, vol. 34, 01 2007.
- [10] E. H. Land and J. J. McCann, "Lightness and retinex theory," *J. Opt. Soc. Am.*, vol. 61, no. 1, pp. 1–11, Jan 1971. [Online]. Available: <http://www.osapublishing.org/abstract.cfm?URI=josa-61-1-1>
- [11] R. Lenka and A. Khandual, "A study on retinex theory and illumination effects–i," *International Journal of Advanced Research in Computer Science and Software Engineering*, vol. 6, 01 2016.
- [12] S. Tang, M. Dong, J. Ma, Z. Zhou, and C. Li, "Color image enhancement based on retinex theory with guided filter," in *2017 29th Chinese Control And Decision Conference (CCDC)*, 2017, pp. 5676–5680.
- [13] Z. Rahman, D. Jobson, and G. Woodell, "Multi-scale retinex for color image enhancement," in *Proceedings of 3rd IEEE International Conference on Image Processing*, vol. 3, 1996, pp. 1003–1006 vol.3.
- [14] X. Fu, Y. Sun, M. LiWang, Y. Huang, X.-P. Zhang, and X. Ding, "A novel retinex based approach for image enhancement with illumination adjustment," in *2014 IEEE International Conference on Acoustics, Speech and Signal Processing (ICASSP)*, 2014, pp. 1190–1194.
- [15] R. C. Gonzalez and R. E. Woods, *Digital Image Processing*. Pearson, 2018, pp. 369–370. [Online]. Available: <https://books.google.co.in/books?id=0F05vgAACAAJ>
- [16] Z. Wang and A. Bovik, "A universal image quality index," *IEEE Signal Processing Letters*, vol. 9, no. 3, pp. 81–84, 2002.
- [17] C. Li, C. Guo, W. Ren, R. Cong, J. Hou, S. Kwong, and D. Tao, "An underwater image enhancement benchmark dataset and beyond," *IEEE Transactions on Image Processing*, vol. 29, pp. 4376–4389, 2020.
- [18] Y. Wang, W. Song, G. Fortino, L.-Z. Qi, W. Zhang, and A. Liotta, "An experimental-based review of image enhancement and image restoration methods for underwater imaging," *IEEE Access*, vol. 7, pp. 140 233–140 251, 2019.



- [19] J. Zhou, D. Zhang, and W. Zhang, “Multiscale fusion method for the enhancement of low-light underwater images,” *Mathematical Problems in Engineering*, vol. 2020, pp. 1–15, 09 2020.
- [20] R. Schettini and S. Corchs, “Underwater image processing: State of the art of restoration and image enhancement methods,” *EURASIP J. Adv. Signal Process*, vol. 2010, Jan. 2010. [Online]. Available: <https://doi.org/10.1155/2010/746052>
- [21] S. Park, B. Moon, S. Ko, S. Yu, and J. Paik, “Low-light image restoration using bright channel prior-based variational retinex model,” *EURASIP Journal on Image and Video Processing*, vol. 2017, 06 2017.
- [22] Y. Gao, H. Li, and S. Wen, “Restoration and enhancement of underwater images based on bright channel prior,” *Mathematical Problems in Engineering*, vol. 2016, pp. 1–15, 11 2016.
- [23] E. Provenzi, L. D. Carli, A. Rizzi, and D. Marini, “Mathematical definition and analysis of the retinex algorithm,” *J. Opt. Soc. Am. A*, vol. 22, no. 12, pp. 2613–2621, Dec 2005. [Online]. Available: <http://josaa.osa.org/abstract.cfm?URI=josaa-22-12-2613>
- [24] M. Tkalcic and J. Tasic, “Colour spaces: perceptual, historical and applicational background,” in *The IEEE Region 8 EUROCON 2003. Computer as a Tool.*, vol. 1, 2003, pp. 304–308 vol.1.
- [25] J. Chen and L.-P. Chau, “An enhanced window-variant dark channel prior for depth estimation using single foggy image,” in *2013 IEEE International Conference on Image Processing*, 2013, pp. 3508–3512.
- [26] W. Hao, M. He, H. Ge, C. jin Wang, and Q.-W. Gao, “Retinex-like method for image enhancement in poor visibility conditions,” *Procedia Engineering*, vol. 15, pp. 2798–2803, 2011, cEIS 2011. [Online]. Available: <https://www.sciencedirect.com/science/article/pii/S1877705811020285>
- [27] Q.-N. Zhao, T.-Z. Huang, X.-L. Zhao, T.-H. Ma, and M.-H. Cheng, “A convex optimization model and algorithm for retinex,” *Mathematical Problems in Engineering*, vol. 2017, pp. 1–14, 07 2017.



- [28] A. A. Reddy, P. R. Jois, J. Deekshitha, S. Namratha, and R. Hegde, “Comparison of image enhancement techniques using retinex models,” *International Journal of Advanced Computer Engineering and Communication Technology (IJACECT)*, vol. 2, 2013.
- [29] A. S. A. Ghani and N. A. M. Isa, “Underwater image quality enhancement through rayleigh-stretching and averaging image planes,” *International Journal of Naval Architecture and Ocean Engineering*, vol. 6, no. 4, pp. 840–866, 2014. [Online]. Available: <https://www.sciencedirect.com/science/article/pii/S2092678216302588>
- [30] W. Song, Y. Wang, D. Huang, A. Liotta, and C. Perra, “Enhancement of underwater images with statistical model of background light and optimization of transmission map,” *IEEE Transactions on Broadcasting*, vol. 66, no. 1, pp. 153–169, 2020.
- [31] W. Song, Y. Wang, D. Huang, and D. Tjondronegoro, “A rapid scene depth estimation model based on underwater light attenuation prior for underwater image restoration,” in *Advances in Multimedia Information Processing – PCM 2018*, R. Hong, W.-H. Cheng, T. Yamasaki, M. Wang, and C.-W. Ngo, Eds. Cham: Springer International Publishing, 2018, pp. 678–688.
- [32] D. Huang, Y. Wang, W. Song, J. Sequeira, and S. Mavromatis, “Shallow-water image enhancement using relative global histogram stretching based on adaptive parameter acquisition,” in *MultiMedia Modeling*, K. Schoeffmann, T. H. Chalidabhongse, C. W. Ngo, S. Aramvith, N. E. O’Connor, Y.-S. Ho, M. Gabbouj, and A. Elgammal, Eds. Cham: Springer International Publishing, 2018, pp. 453–465.